

Transferable atomistic model to describe the energetics of zirconia

Mark Wilson, Uwe Schönberger, and Michael W. Finnis*

Max-Planck-Institut für Metallforschung, Institut für Werkstoffwissenschaft, Seestrasse 92, D-70174 Stuttgart, Germany

(Received 1 February 1996; revised manuscript received 1 April 1996)

We have investigated the energies of a number of phases of ZrO_2 using models of an increasing degree of sophistication: the simple ionic model, the polarizable ion model, the compressible ion model, and finally a model including quadrupole polarizability of the oxygen ions. The three structures which are observed with increasing temperatures are monoclinic, tetragonal, and cubic (fluorite). Besides these we have studied some hypothetical structures which certain potentials erroneously predict or which occur in other oxides with this stoichiometry, e.g., the $\alpha\text{-PbO}_2$ structure and rutile. We have also performed *ab initio* density functional calculations with the full-potential linear combination of muffin-tin orbitals method to investigate the cubic-tetragonal distortion. A detailed comparison is made between the results using classical potentials, the experimental data, and our own and other *ab initio* results. The factors which stabilize the various structure are analyzed. We find the only genuinely transferable model is the one including compressible ions and anion polarizability to the quadrupole level. [S0163-1829(96)00334-7]

I. INTRODUCTION

ZrO_2 is an important industrial ceramic combining high-temperature stability and high strength.¹ It is used as an oxygen sensor, in fuel cells, O_2 pumps, and as susceptors for induction heating, as well as artificial diamonds. In order to understand its properties and predict them there is a need for atomic scale simulation, which requires a reliable model for the energy and interatomic forces. Such a model should be transferable between different crystal structures and physical conditions. The wide range of applications, particularly those at high temperature, makes the derivation of a *transferable atomistic model* especially important because experimental measurements of material properties at elevated temperatures are difficult to perform and are susceptible to errors caused by the extreme environment. First principles, or *ab initio* calculations, which are based on solving the Kohn-Sham or Hartree-Fock equations for the electronic structure, give the most reliable information about properties, but they are only possible for very simple structures involving a few atoms per unit cell. For example, they have been used to map the energy for the tetragonal-to-cubic phase transformation;^{2,3} but even the perfect ground-state monoclinic structure would require for an *ab initio* treatment computer power beyond what is presently available to most laboratories. An atomistic model which can be used to investigate properties of complex structures at all temperatures and pressures is the goal of this paper.

Previous work in this direction has been based on the ionic model, extended by including polarizable ions—the shell model.⁴ The starting point for our present model is also an ionic description; that is, ZrO_2 is treated as Zr^{4+} and O^{2-} ions, which we extend by using a polarizable-ion model (PIM),⁵ which has been shown to give a better description of the underlying physics than the old shell model,⁴ but with the additional features of compressible ions and quadrupolar distortions. We found the original shell model to be inadequate to account for the observed crystal structures of ZrO_2 . In order to keep our development physically motivated, we ex-

amine carefully the effect of polarizable ions on the energetics of different crystal structures. It is useful to start by considering how the rigid ions may pack together as hard spheres. This will set the scene for understanding the observed structures in ZrO_2 .

Although the prediction of crystal structures using radius-ratio rules is not so well justified for oxides as for halides, because the anion volume depends more on the specific crystalline environment,⁶⁻⁸ it is possible to look at *trends* in terms of the cation radii as these are generally well defined and transferable between different crystal structures. The general rule, that the larger the cation the larger the cation-anion coordination number, still applies despite the expected fluctuations in the anion volume. Table I shows a structure map for a range of systems with stoichiometry MO_2 . The smallest cations (Si and Ge) form four-coordinate silicalike structures based on corner-linked MO_4 tetrahedra. The “medium”-sized cations tend to form the six-coordinated rutile structure while the larger (actinide) cations form the eight-coordinate fluorite structure. Both ZrO_2 and HfO_2 have a seven-coordinate monoclinic structure as their ground state. In terms of coordination number it is intermediate be-

TABLE I. MO_2 structure map. The smallest cation (Si^{4+}) is at the top with the largest (actinide) cations at the bottom.

Ion	Structure	Cation Coordination Number
Si	Silica	4
Ge	Silica	4
Ti	Rutile	6
Sn		
Pb		
Zr	Monoclinic	7
Hf	Monoclinic	7
U	Fluorite	8
Th		
Ce		

tween the rutile and the fluorite structures. The cations appear too large to form an efficiently packed rutile structure but too small for the fluorite structure to be energetically favorable. In fact there is a fluorite structure for ZrO_2 at higher temperature, as discussed below, but if its coordinates are extrapolated to 0 K, the O-O nearest-neighbor separation is short compared to those observed in oxides with fluorite ground state.⁹

The rutile and fluorite structures are relatively efficient in terms of the packing of the respective sublattices in order to maximize anion-cation interactions and minimize the high-energy cation-cation interactions. The cations occupy holes such that the cation-cation nearest-neighbor separation, r_{++}^{NN} is greater than the anion-anion analog r_{--}^{NN} . The driving force is the greater cation charge which results in a greater cation-cation Coulombic repulsion (whose energy goes as the cation charge squared) with respect to the anion-anion repulsions. As a result these systems can be termed *charge ordered*. There is no simple seven-coordinate structure that allows for such efficient packing. This simple analysis, based essentially on packing charged spheres of appropriate radius, points to the structure of ZrO_2 (and HfO_2) being determined by a more subtle balance of effects than may be the case in the rutile or fluorite MO_2 systems.

Further evidence for this subtle balance of effects lies in the rich and varied structures taken by both ZrO_2 and HfO_2 with increasing temperature and pressure. On increasing the temperature both systems change their structure in the sequence monoclinic (7 coordinate cations) \rightarrow tetragonal (≈ 8 coordinate cations) \rightarrow fluorite (8 coordinate) prior to melting.¹ Evidence is increasing that with increasing pressure both form two phases with orthorhombic symmetry:¹⁰⁻¹⁶ a low-pressure orthorhombic phase closely related to the monoclinic and a higher-pressure phase with a distorted cotunnite (PbCl_2) structure.

We now describe in detail the structures which are important for ZrO_2 . In fluorite, the stable structure above 2000 K, the eight-coordinate cations form a fcc lattice with the anions occupying all the available tetrahedral holes. The tetragonal structure is stable down to 1200 K when cooled and up to 1450 K when heated¹⁷ and can be derived from the cubic via appropriate shifts in lines of anions. This shift is accompanied by an increase of the c/a ratio from $\sqrt{2}$ for the perfect cube to ≈ 1.45 .

We also consider the rutile structure as the structure map of Table I indicates that both ZrO_2 and HfO_2 are *intermediate* between rutile and fluorite in terms of cation size. Here, the anions form a distorted close-packed lattice with the cations in the octahedral holes. An alternative viewpoint is to consider this structure as an array of edge- and corner-linked MO_6 octahedra.¹⁸ Figure 1 shows the experimental monoclinic ground-state structure which is stable below 1200 K. This structure is often described in terms of distortions from the fluorite structure (see, for example, Ref. 19). An alternative viewpoint is to consider the structure as alternating layers of fluoritelike (four-coordinate) and rutilelike (three-coordinate) oxide anions (labeled O^{I} and O^{II} , respectively, in the diffraction work²⁰⁻²²), highlighted in the figure by the two different shades of grey for oxygen sites. The intermediate nature of the monoclinic structure is further confirmed by considering the nearest-neighbor anion-cation separations

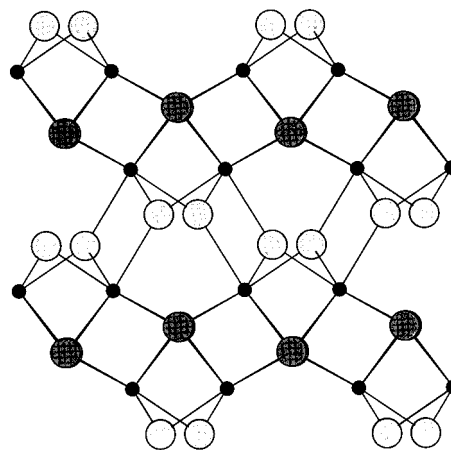


FIG. 1. Monoclinic crystal structure. Key: large spheres, O^{2-} ; small, Zr^{4+} . The darker large spheres distinguish the four-coordinate oxides from the three-coordinate oxides shown in a lighter grey.

in this structure and in the rutile and fluorite at their respective energy minima. The three-coordinate anion-cation separations (2.05, 2.06, and 2.16 Å, respectively,²⁰) are close to the equilibrium rutile separation (2.12 Å) and the four-coordinate anion-cation separations (2.15, 2.19, 2.20, and 2.29 Å) are similar to the fluorite separation (2.24 Å). Finally, we also consider the orthorhombic $\alpha\text{-PbO}_2$ structure.¹⁸ Although this structure is not observed experimentally for ZrO_2 or HfO_2 , every shell model known to us gives it as the ground state. It consists of distorted MO_6 octahedra edge sharing to form zigzag chains. The displacement of the cation, within the local octahedron of anions, away from the perfect octahedral symmetry site, brings a further two anions to within what can be considered as the first coordination sphere, giving an overall 6+2 coordination. These extra anions lie beyond the distorted anion octahedra and are associated with two *different* nearest-neighbor cation octahedra. Zr^{4+} has a larger ionic radius (0.80 Å) than Ti^{4+} (0.68 Å),²³ and rutile (TiO_2) can be transformed to an $\alpha\text{-PbO}_2$ structure by applying pressure.¹⁸ Hence it is not so surprising that the $\alpha\text{-PbO}_2$ structure is found to be the shell-model ground state for ZrO_2 . Since the $\alpha\text{-PbO}_2$ structure is still based on the linking of MO_6 octahedra, we shall refer to it as being six-coordinate rather than 6+2 since the two extra anions are significantly further away from the central cation.

From the above discussion it is clear that *both* the monoclinic (seven-coordinate) and the $\alpha\text{-PbO}_2$ structures lie in an “intermediate” region between the six-coordinate rutile and the eight-coordinate fluorite. An important task of this paper is therefore to unravel the physics which stabilizes the monoclinic structure with respect to the $\alpha\text{-PbO}_2$. This clearly involves going beyond the simple ionic models, and is an essential step to deriving a transferable model for ZrO_2 .

There have been several previous attempts to construct an atomistic model for ZrO_2 in the form of an effective pair potential (EPP) plus dipole polarizabilities. Boyer and Klein²⁴ derived a simple rigid-ion potential from linear muffin-tin orbital (LMTO) *ab initio* calculations. The resulting potential model gives the cubic (fluorite) structure as the

ground state, implying that polarization effects need to be included which will act to lower the energy of the lower-symmetry structures compared to the highly symmetric fluorite polymorph.

The shell-model potential of Dwivedi and Cormack (DC),²⁵ derived from the experimental tetragonal structural parameters and the dielectric constant, does give a lower energy for the monoclinic structure with respect to the cubic. A more recent shell-model potential¹⁹ is very similar in form to the DC potential. However, we found by relaxing the crystal structure with the GULP program²⁶ that the monoclinic structure is not the ground state with this potential, which favors instead the α -PbO₂ structure.

Perhaps the state-of-the-art paper concerning ZrO₂ is that of Stefanovich *et al.*¹⁹ who present an interesting mix of calculation techniques including Hartree-Fock,²⁷ semiempirical Hartree-Fock,²⁸ and atomistic relaxation with classical potentials.²⁶ The full Hartree-Fock calculation reproduces many of the observed experimental properties including the monoclinic ground state. The semiempirical method gives a less satisfactory representation. The classical model predicts the α -PbO₂ structure to be the ground state.

The *potential-induced breathing model*^{29,30} (PIB) augments the EPP by allowing for the spherical relaxation (“breathing”) of the oxide anion charge density, calculated using a Watson sphere method. Importantly, the energy differences between the various polymorphs are different in comparison to the EPP models which indicates that an EPP alone is not transferable.

More *ab initio* data are available concerning the tetragonal-cubic transition than for any other aspect of ZrO₂. Experimental information is available at high temperatures (>1200 °C),¹⁷ while the *ab initio* data concentrate on zero K structural information. In this respect, therefore, the *ab initio* and experimental data can be considered as complementary.

We summarize here the results of different *ab initio* calculations and compare them to experiment. The full-potential linearized augmented-plane-wave (FLAPW) *ab initio* calculations of Jansen,² based on density functional theory in the local-density approximation (LDA), give $d_z=0.029$, while Hartree-Fock calculations (the CRYSTAL code) give $d_z=0.0246$ (Ref. 19) (both at zero K). Our own LMTO calculations (another standard LDA method), studying a range of unit cell volumes, give d_z in the range 0.02–0.04. The volumes cover the range from $V/V_0=0.92$ to $V/V_0=0.98$, where V_0 is the volume of minimum energy at 0 K for the fluorite structure. Experimental neutron scattering¹⁷ gives d_z between 0.0574 at 1568 K and 0.0605 at 2318 K. The experimental data are somewhat ambiguous in the sense that, although d_z falls with temperature, the values at 1768 and 1568 K are identical to within the error of the experiment. On the basis of these data one might either argue for d_z tending to ≈ 0.057 at 0 K or argue for a linear decrease to ≈ 0.04 by extrapolating from the higher-temperature data. However, if one supposes that the *ab initio* data would agree with experiments extrapolated to 0 K, then the “linear decrease theory” seems the most plausible.

The LDA ($T=0$ K) calculations give a value of 1.425 for the c/a ratio at the energy minimum,² close to the Hartree-Fock value of 1.421.¹⁹ The high-temperature experimental

value is around 1.45 with a maximum at $\approx 1700^\circ\text{C}$.¹⁷ The shell model ($T=0$ K) gives a value of 1.454 in good agreement with the *high-temperature* data.¹⁹

The experimental value for the energy barrier ΔU^{tet} in the double well at the transition temperature is 0.057 eV (4.19 mRy).³¹ Hartree-Fock calculations give 0.008 eV (Ref. 19) as does LDA calculations.²

The published shell model of Stefanovich *et al.*¹⁹ predicts a tetragonal distortion with $d_z=0.060$ at $T=0$ K. This is in excellent agreement with the *high-temperature* experimental data but in poorer agreement with the *ab initio* $T=0$ K data.

The extent of the task we have set ourselves in this paper, therefore, is to derive a model suitable for use in molecular dynamics simulations, which not only reproduces the monoclinic structure as the ground state, but also reproduces the other properties without further modification of the basic model parameters. The complex nature of the ZrO₂ morphology should provide a stern test of the true *transferability* of such a potential model.

Having suggested that it is necessary to go beyond the physics traditionally represented by the shell model, our first step is to include the breathing of the oxide ion, the second step is to include dipolar induction effects, and the third step quadrupolar induction. Our formal procedure is described in Sec. III, after the following more detailed analysis of the problems inherent in modeling oxides. The plan of the rest of the paper is as follows. In Sec. IV we describe how our model parameters are specified. In Sec. V we present results for the energy-volume curves for the various structures, as well as calculated lattice parameters and elastic constants. We also describe results for the energy versus tetragonal distortion, for which Jansen² and ourselves have performed *ab initio* calculations for comparison. A general discussion of our results is presented in Sec. VI and in Sec. VII we conclude.

II. PROBLEMS OF SIMULATING OXIDES

In this section the specific problems associated with simulating oxides will be outlined. O²⁻ is unstable in the free state with respect to decomposition to O⁻ and an electron: The anion is effectively infinitely polarizable. In the condensed environment the Madelung potential stabilizes the addition of the second electron to O⁻.^{7,32} As a result the nature of the anion (its volume and polarizability) is much more dependent upon the specific environment than for, say, the halides which, although also compressed by the crystalline environment, are stable in the free state. This insensitivity of the halide anion to the precise nature of the ionic environment allows simple EPP’s to be used with great success over a relatively wide range of coordination environments. For O²⁻ the dependence of the anion volume on environment must be included in the model.

Our starting point is the *ab initio* investigation of environmental effects in cubic crystals by Pyper.^{33,34} The short-ranged interatomic repulsion energy at a lattice parameter R , $U^{\text{SR}}(R)$, is decomposed into a rearrangement (or self-) energy [$U^{\text{re}}(Z;R)$] and an overlap energy [$U^{\text{ov}}(R)$]

$$U^{\text{SR}}(R) = U^{\text{re}}(Z;R) + U^{\text{ov}}(R). \quad (2.1)$$

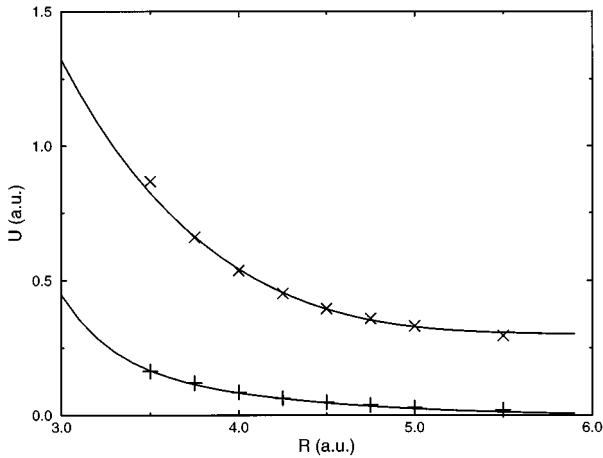


FIG. 2. ZrO_2 *ab initio* (points) and fits (solid lines). Key: \times – $U^{\text{re}}(4;R)$; $+$, $U^{\text{ov}}(R)$.

$U^{\text{re}}(Z;R)$ is the energy to create the anion with the charge density appropriate to the crystal at lattice parameter R in a crystal with coordination number Z and is calculated by solving for the self-consistent wave function and energy of the anion in a confining potential which simulates the crystalline environment at lattice constant R . The confining potential includes both a lattice of point charges (“Madelung potential”) and a pseudopotential which mimics the repulsion of the electrons by the closed-shell charge densities of the neighboring cations, both spherically averaged about the anion position. Both potentials serve to compress the anion relative to its free state.^{35,36} $U^{\text{ov}}(R)$ then results from the overlap between the optimized wave functions summed over pairs of ions. The model fitted to *ab initio* data in this form is termed the *compressible-ion model* (CIM).³⁷

Figure 2 shows the results of such a calculation for ZrO_2 in the fluorite structure.³⁸ For the fluorite structure there are four overlap contributions per single rearrangement energy term. The rearrangement energy goes to a finite value at $R=\infty$ which corresponds to the energy required to form a (hypothetical) free O^{2-} ion from O^- and an electron.

In order to help us to clarify why this representation is expected to give a better description of those properties which depend on coordination number, we derive an EPP from the *same ab initio* data. In the fluorite structure the crystal energy is given by

$$U^{\text{SR}}(R) = \sum_{i=2}^{N_t} \sum_{j=1}^{i-1} U^{\text{EPP}}(r^{ij}) = \frac{1}{4} [U^{\text{re}}(4;R) - U^\infty] + U^{\text{ov}}(R), \quad (2.2)$$

where the factor of $\frac{1}{4}$ is included to cancel the summation over nearest neighbors. The *ab initio* data can now be used to fit with the usual Born-Mayer-type exponential function. An analogous fitting procedure carried out using a crystal structure with a different coordination number may, however, yield a different curve (and hence require different Born-Mayer parameters), reflecting the fact that U^{re} and U^{ov} depend differently on coordination number.³⁹ The transferability of an effective pair potential model relies on the short-range interactions being primarily due to the overlap between *frozen* charge densities. In reality, the differing de-

pendences of the rearrangement and overlap energies on the coordination number means that a *single* EPP is inappropriate over a range of coordination numbers. This problem is expected to be particularly acute for oxides (and, indeed, any anion whose existence in the condensed phase depends on the confining potential; other examples include the chalcogenides and N^{3-}). However, the same problems do arise in halides in a more subtle form.⁴⁰

III. MODEL STRATEGY AND FORMALISM

As demonstrated in the previous section, EPP and CIM representations can be generated from *ab initio* data and compared for the various experimentally observed and imagined structures. Polarization effects, to the desired order, can also be included in an identical manner in the two short-range formalisms. We anticipate that, given the relative complexity of the outlined problem coupled with the shortcomings of previous empirical models, the best strategy is to consider models of *varying complexity* but parametrized from the same *ab initio* data. This will shed light on the subtle balance of physical effects required to reproduce the experimentally observed trends.

The total energy for the CIM is partitioned into the following components:

$$U^{\text{tot}}(R) = U^{\text{re}}(Z;R) + U^{\text{ov}}(R) + U^{\text{disp}}(R) + U^{\text{ind}}(R) + U^{\text{Coul}}(R). \quad (3.1)$$

U^{re} and U^{ov} have been described above. U^{Coul} is simply the energy of interaction of the (formally charged) ions ($U^{\text{Coul}} = \sum_{i=2}^{N_t} \sum_{j=1}^{i-1} Q^i Q^j / r^{ij}$). U^{ind} is the total induction energy including multipoles induced to the desired order (in this case dipolar or dipolar plus quadrupolar). Details of the induction models will be presented later in this section. Finally, U^{disp} is the dispersion energy given in general by

$$U^{\text{disp}} = \sum_{n=6,8}^{\infty} \sum_{i=2}^{N_t} \sum_{j=1}^{i-1} \frac{C_n^{ij}}{r^{ijn}} f_n(r^{ij}), \quad (3.2)$$

where C_n is the appropriate dispersion coefficient and f_n is the dispersion damping function representing the effect of the overlap of the electron clouds, acting to reduce the dispersion interaction from its asymptotic value.

In the CIM,³⁷ the breakdown of the anion-cation short-range energy into the rearrangement and overlap parts has been formulated in a way which is suitable for performing molecular dynamics simulation. The internal state of an ion depends on the change δ^i in its radius $\bar{\sigma}^i$, leading to a total short-range energy given by

$$U^{\text{SR}} = \sum_{j < i} u_{\text{CIM}}^{ij} [r^{ij} - (\bar{\sigma}^i + \delta^i) - (\bar{\sigma}^j + \delta^j)] + F(\delta^i), \quad (3.3)$$

where u_{CIM}^{ij} is the pair overlap term and $F(\delta^i)$ is the rearrangement energy. At the self-consistent energy minimum for a given set of ion coordinates $\{r^i\}_{i=1,N}$, U^{SR} is minimized to determine the adiabatic ion radii given by $\{\delta_{\text{opt}}^i\}_{i=1,N}$.

For ZrO_2 *ab initio* data are available for the fluorite (four-coordinate anion) phase. The parameter set

$\{A^{+-}, B^{+-}, C^{+-}, D, a^{+-}, \gamma\}$ (in the notation of Ref. 37) is adjusted to satisfy the condition

$$E_{\text{ov}}(R) + E_{\text{re}}(R) = F(\delta_{\text{opt}}) + 4u_{\text{CIM}}^{+-}(R, \delta_{\text{opt}}) \quad (3.4)$$

over the range of lattice parameters R used in the *ab initio* calculations. δ_{opt} minimizes the total energy determined from

$$\left(\frac{\partial U}{\partial \delta}\right)_R = 4\left(\frac{\partial u_{\text{CI}}^{+-}}{\partial \delta}\right)_R + \left(\frac{\partial F}{\partial \delta}\right)_R = 0, \quad (3.5)$$

which is solved by the bisection method.⁴¹ Note that this condition leads to the total energy having a many-body character despite only requiring pair separations for its evaluation.

Induced point dipoles are included as additional degrees of freedom in an extended Lagrangian formalism^{42,5} using a polarizable-ion model (PIM) in which molecular dynamics are performed using ideas borrowed from the Car-Parrinello (CP) method⁴³ in the manner of Sprik and Klein.⁴² Hartree-Fock electronic structure calculations on distorted LiF crystals⁴⁴ demonstrate that the short-range (overlap) induced dipoles can be viewed as the result of an additional potential (dubbed the ‘‘dent-in-the-wall’’ term). To study the induced anion dipole a single cation was displaced from the anion first-coordination sphere. The resulting dipole moment could then be decomposed into the Coulombic and overlap terms. The overlap term was shown to be approximately additive and is included in the model via the Tang-Toennies damping function, $f^{(1)}$.⁴⁵ This function has a single parameter b^{an} [the short-range damping parameter (SRDP)], which goes as the reciprocal of the length scale over which the overlap damping acts.

Overall, therefore both a polarizability and the SRDP are required to complete the dipolar PIM.

An advantage of including induction effects in the above manner is that the extension to higher-order moments is more natural than in the more traditional shell model. To this end the basic dipolar model has been extended to study both the effects of cation quadrupoles [in AgCl (Ref. 46)]. The alterations to deal with anion moments are mathematically simple.

IV. PARAMETRIZATION

Having derived computationally tractable models to describe the response of the oxide ion to the ionic environment (the ‘‘breathing’’ of the anion) and to handle induced moments within a dipolar or quadrupolar approximation, we now consider how each part of the model may be most effectively parametrized.

A. Short-range terms

As stated in the Introduction, the starting point for the models is a basic ionic description. Formal ionic charges, the full valence charges, rather than partial charges as some authors have used, are adopted here for three basic reasons. First, both the *ab initio* calculations (used to derive the short-range parameters) and the polarizabilities assume full valence charges. The use of partial charges would, therefore, require a full reanalysis of all other terms in the potential

TABLE II. Fitted CIM parameter sets for ZrO_2 in the notation of Ref. 37.

Parameter/a.u.	
a^{+-}	1.70
A^{+-}	160.0
B^{+-}	300 000.0
C^{+-}	0.0
γ	1.56
D	0.1505
ϵ	3.5
E	9200.0

model. Second, it appears to us that the use of full formal charges, coupled with a physically based description of induction effects, presents the best chance of deriving empirical models that are truly *transferable* over a range of state points. The use of partial charges, the values of which are not physically well defined, tends to restrict the applicability of potential models to specific statepoints. Third, the use of the full formal charges allows a direct comparison between the potential model and the experimental thermophysical quantities subject to the problems in interpreting the second electron affinity of the oxide anion discussed in Sec. II.

The CIM is fitted to the *ab initio* calculations as shown in Fig. 2, with the model parameters given in Table II. The EPP is derived from the same *ab initio* data by fitting a Born-Mayer exponential function to Eq. (2.2). $U^{\text{re}}(Z; \infty)$ must be added back to energies derived from the EPP model for comparison with the CIM. The EPP fit is shown in Fig. 3 along with previous EPP model curves²⁵ for comparison. The current EPP appears very similar to the previous potentials (derived from purely empirical considerations) in shape although it is consistently more repulsive at a given ion separation. The EPP parameters are given in Table III.

The similarity of the current EPP to the empirical potentials highlights an important point. A possible interpretation of the failure of the empirical models is that it is purely a parametrization problem; that is, given the right parameter set the shortcomings would disappear. However, the similarity of the *ab initio* curves to the current *empirical* models indicates that this is not the case and points towards significant physical effects being absent from these simple models.

Table IV compares the zero K lattice parameter predicted by *ab initio* calculations³⁸ (and hence predicted by both the CIM and EPP) with previous calculations and two experimental values. The experimental values are derived from extrapolation from two different sources: from the high-temperature neutron scattering data¹⁷ and to zero impurity in the cubic stabilized structure.⁴⁷ As a result of these extrapolation procedures both experimental values are subject to significant errors. The current predicted lattice parameter is larger than both experimental values and in best agreement with the Hartree-Fock calculation.¹⁹

B. Polarization terms

The polarizabilities of the individual species (Zr^{4+} and O^{2-}) are deduced as 2.756 and 14.872 a.u.,⁴⁸ respectively, from the molar polarizability obtained from experimental di-

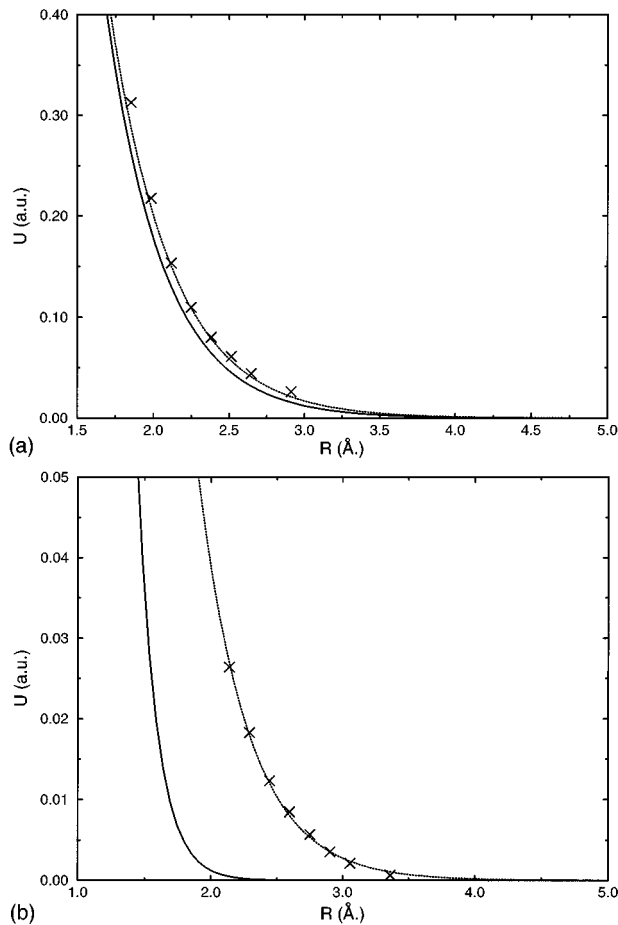


FIG. 3. Pair potentials: (a) Zr-O, (b) O-O. Key: X, *ab initio* data (Ref. 38). Dotted line, fit to the *ab initio* data. Solid line, previous empirical potential (Ref. 25).

electric properties⁴⁹ and a polarizability obtained for O^{2-} by extrapolation of *ab initio* calculations on other oxide systems.⁴⁸ Additional confidence in the extraction of the individual ion polarizabilities comes from relativistic coupled Hartree-Fock calculations⁵⁰ on the gaseous Zr^{4+} ion which give a polarizability of 2.98 a.u. In comparing the Hartree-Fock value with the number obtained from the experimental molar polarizability it is assumed that the nature of the Zr^{4+} cation is unaffected by the crystalline environment⁵¹ as demonstrated for the alkali and alkaline-earth oxides⁶ and so the condensed phase polarizabilities are unchanged from the gas phase values.

The model may be simplified (and hence made computationally more efficient) by treating the Zr^{4+} cations as rigid, that is, of zero polarizability. This can be justified on two

TABLE III. Dipole-dipole (C_6) and dipole-quadrupole (C_8) dispersion terms from Ref. 48 with Tang-Toennies damping function parameters.

	$C_6/a.u.$	b^{SR}	$C_8/a.u.$	b^{SR}	$a/a.u.$	$B/a.u.$
Zr-O	25.183	2.201	307.24	2.411	1.30	27.25
O-O	90.79	2.251	1391.08	2.302	1.40	7.72
Zr-Zr	9.274	2.511	84.19	2.674	-	-

TABLE IV. *Ab initio* 0 K fluorite lattice parameters compared with experimental values.

Method	$a_0/\text{Å}$	$V/\text{Å}^3$	Ref.
CLUSTER	4.940	30.14	19
CRYSTAL	5.154	34.23	19
FLAPW-DFT	5.03 ^a	32.27	2
Hartree-Fock	5.035	31.91	3
Potential-induced breathing	5.101	33.19	30
LMTO	5.04	32.90	Current work
RIP	5.162	34.39	38
Expt.	5.090	32.97	17
Expt.	5.127	33.69	47

^aEstimated from Fig. 2 in Ref. 2.

fronts; first, the bare polarizabilities quoted above satisfy $\alpha_{Zr^{4+}} \ll \alpha_{O^{2-}}$ and second the anion finds itself in a stronger electric field as a result of the larger charge of the nearest-neighbor cations.

Finally, for the dipolar model, a SRDP is required. Following previous work³⁷ a value of 1.7 a.u. is chosen.

The model is now complete to within the dipolar approximation. As might be expected, the parametrization of the quadrupolar parts of the model is more problematic. Ideally, one would be able to call upon the relative wealth of *ab initio* data available to parametrize the dipolar induction effects. Unfortunately the sorts of electronic structure calculations required are, as yet, relatively sparse.⁵² As a result the parametrization of the quadrupolar interactions will be simplified as much as possible.

The full model requires a quadrupole polarizability C , a dipole-dipole-quadrupole hyperpolarizability B , and an overlap function $f^{(2)}(r)$.⁴⁶ An analogous analysis to that used in the dipole case indicates that the overlap-induced quadrupole will act *against* the Coulombic-induced moment—the overlap damps the Coulombic induction. Information regarding the magnitude of this interaction again comes from the same series of *ab initio* Hartree-Fock calculations on distorted crystals on LiF used for the dipolar model.⁴⁴ These show that the overlap interaction effectively cancels that induced by the Coulombic interactions. This observation perhaps makes clear why anion quadrupolar effects have not been found to be necessary more generally. In ZrO_2 , however, the magnitudes of the energy differences between possible crystalline phases are such that small anion quadrupole effects may be significant. Additionally, in the crystalline environment the high symmetry of the anion site may more effectively cancel the induced dipoles (which would be expected to dominate in more asymmetric liquid environments), projecting the anion quadrupoles to a greater level of importance.

No direct *ab initio* C is available for O^{2-} in ZrO_2 . Sen and co-workers^{53,54} have derived an approximate relationship linking α and C which, coupled with the known *ab initio* α for ZrO_2 of 14.872 a.u.,³⁸ gives $C = 61.86$ a.u. Following previous work on $AgCl$,⁴⁶ B can be approximated via the relationship $B \approx -6C$.

However, even with this approximate C and B parameter set we are still lacking real information to effectively derive the function $f^{(2)}$. An alternative strategy is to consider the Coulombic- and overlap-induced quadrupoles together. If we

had a suitable range of *ab initio* calculations, then the C and B values would be those relating to the electrostatic-induced moments only with the $f^{(2)}$ function parametrized from distorted crystal calculations in an analogous fashion to the dipole model.⁵ In the absence (as yet) of such a range of *ab initio* calculations one option is to set the $f^{(2)}$ function to unity and use a C (and hence B) that is smaller than that predicted for the purely electrostatic interactions, thus mimicking the opposing Coulombic and overlap effects. The quadrupolar model described above is complete in the sense that it allows for both the Coulombic and overlap moments to be included in a well-defined way. However, it seems inappropriate to derive an $f^{(2)}$ function from very little data in order to oppose a Coulombic moment dependent upon a quadrupole polarizability that is also poorly defined. The magnitude of the available quadrupole polarizabilities lead us to believe that a quadrupole polarizability of 9–12 a.u. will be appropriate for ZrO_2 .

The fact that the rest of the potential model is well defined in terms of the connection of each term in the energy partition to *ab initio* calculations allows C to be varied independently of these terms and so its effect on the energetics can be closely investigated. The value of B is connected to C as described above and never varied independently.

C. Other potential terms

Having obtained accurate values for the individual ion polarizabilities Fowler *et al.*⁴⁸ derived dipole-dipole (C_6) and dipole-quadrupole (C_8) dispersion coefficients from the Slater-Kirkwood⁵⁵ and Starkschall-Gordon⁵⁶ formulas, respectively. Dispersion damping is included via Tang-Toennies functions⁴⁵ fitted to more complex functions.^{34,57} These values are given in Table III.

Following previous CIM work³⁷ a frozen $\text{O}^{2-}-\text{O}^{2-}$ potential is used derived from *ab initio* calculations at varying lattice parameters using the oxygen anion electron density calculated at the equilibrium lattice parameter throughout. The *ab initio* results³⁸ are shown in Fig. 3 along with the fit to the usual Born-Mayer exponential (Table III). For comparison the (almost hard-sphere-like) potential used in the previous empirical models is shown.^{19,25} The current *ab initio* potential is much more repulsive and longer ranged than the older, empirical, model. Although the short-range interaction energy for the nearest-neighbor $\text{O}^{2-}-\text{O}^{2-}$ separations is much smaller than the corresponding Coulombic interaction, the greatly differing curvature of the different short-range terms strongly affects the crystal properties.

V. CALCULATIONS

The lattice energies of the various polymorphs are calculated using the EPP and CIM representations of the anion-cation short-range forces. In order to try to fully understand the effect of the anion compressibility and the polarization effects the EPP will be compared with the CIM *without* polarization effects. First, dipole effects and then dipole plus quadrupole polarization effects will be added in an attempt to understand how each term affects the relative polymorph energetics.

Since more *ab initio* data are available for the tetragonal

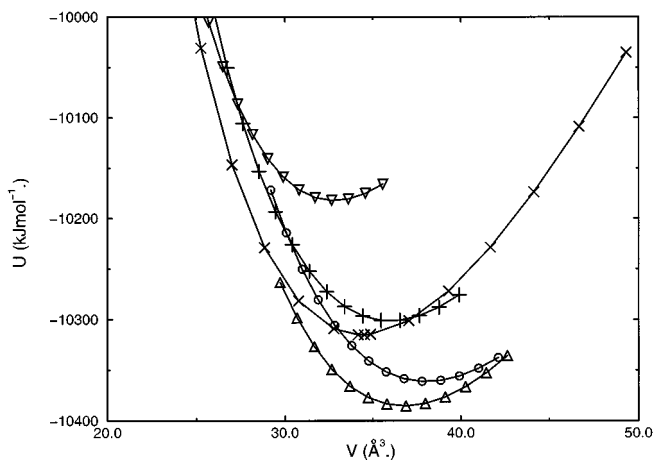


FIG. 4. Lattice energy vs volume for the current EPP. Key: \times , fluorite; $+$, monoclinic; \circ , rutile; ∇ , cotunnite; Δ , α - PbO_2 .

phase, a set of detailed calculations has been made for this structure. Static energy minimizations were carried out at nine unit cell volumes with six c/a ratios (1.48, 1.46, 1.45, 1.44, 1.42, 1.40) at each volume. At each volume and c/a ratio minimizations were performed at ten tetragonal displacements.

A. Effective pair potential

To fully understand the current EPP it is compared with the empirical DC model and an EPP (EPP-OO) in which the $\text{O}^{2-}-\text{O}^{2-}$ short-range term is neglected. The purpose of this second EPP is simply to clarify the role of the anion-anion short-range term.

Figure 4 shows the crystal energies against volume for the current EPP. The energetic order is $U^{\alpha-\text{PbO}_2} < U^{\text{rutile}} < U^{\text{fluorite}} < U^{\text{monoclinic}} < U^{\text{cotunnite}}$ compared with $U^{\alpha-\text{PbO}_2} < U^{\text{fluorite}} < U^{\text{rutile}} < U^{\text{monoclinic}} < U^{\text{cotunnite}}$ for the DC model. The current potential favors the rutile structure over the fluorite.

This change in ordering can be traced directly back to the difference in the $\text{O}^{2-}-\text{O}^{2-}$ short-range potential. In our EPP this term is much more significant at relevant $\text{O}^{2-}-\text{O}^{2-}$ separations than in the DC model (as shown in Fig. 3). For example, at the energy minimum for the fluorite structure the DC potential oxide-oxide short-range energy is some two orders of magnitude less than that for the current EPP. The general effect of this increase in significance of the anion-anion short-range term is to destabilize the higher-coordinate structures. In confirmation EPP-OO reproduces the energetic order of the DC potential—the small difference in the $\text{Zr}^{4+}-\text{O}^{2-}$ repulsive term is not large enough to change the relative energetics of these crystals. Table V lists the energy differences between the polymorph energy minima and the volumes.

The lower symmetry of the O^{2-} sites in the monoclinic phase allows dipoles to be induced that lower the energy in comparison to the fluorite structure. In the fluorite structure the O^{2-} sites have cubic point symmetry, which means they cannot have dipole moments. As a result the full shell model does stabilize the monoclinic phase over the fluorite as does the current EPP with dipoles only.

TABLE V. Energy minimum volumes (in \AA^3) per molecule for the pair potentials.

Structure	$V/\text{\AA}^3$			$\Delta U/\text{kJ mol}^{-1}$		
	DC	EPP (full)	EPP-OO	DC	EPP (full)	EPP-OO
Fluorite	32.81	34.39	31.80	-	-	-
Monoclinic	34.72	35.99	33.53	45.0	13.7	44.6
Rutile	37.23	38.04	35.84	17.2	-46.0	15.7
Cotunnite	30.93	32.69	30.28	123.0	125.3	125.5
αPbO_2	35.17	36.82	34.02	-16.7	-70.5	-21.7

In both the current EPP and DC models both the rutile and the $\alpha\text{-PbO}_2$ phases have a lower-energy minimum than either the monoclinic or the fluorite structures. The difference in the rutile/ $\alpha\text{-PbO}_2$ energetics can again be traced back to the more significant $\text{O}^{2-}\text{-O}^{2-}$ short-range term used in the current work.

The most striking aspect of these potentials is that the $\alpha\text{-PbO}_2$ structure is the ground state regardless of the details of the potential (confirming the previous findings¹⁹). There seems to be no simple way of modifying these potentials to lower the energy of the experimentally observed monoclinic phase with respect to the $\alpha\text{-PbO}_2$.

If we take the experimental enthalpy of formation and apply the Born-Haber cycle²³ for the monoclinic ground state at 298 K, we get a lattice energy, with respect to the Zr^{4+} and O^{2-} ions, of $-11\,060\text{ kJ mol}^{-1}$. All of the pair potentials studied give energies for their respective ground states which are less negative than this.

Table VIII lists the elastic constants (C_{11} , C_{12} , and C_{44}) for the fluorite structure along with the bulk modulus B and experimental values. B is obtained from the isotropic expansions and compressions of the cell. The shear modulus $C_s [\equiv \frac{1}{3}(C_{11} - C_{12})]$ is calculated via an expansion (contraction) along the 100 direction with a volume-conserving contraction (expansion) perpendicular to this.⁵⁸ A knowledge of $B [\equiv \frac{1}{3}(C_{11} + 2C_{12})]$ and C_s yields the values for C_{11} and C_{12} . C_{44} is calculated by applying a shear in the 100 direction.⁵⁸ The bulk modulus and elastic constants agree fairly well with experiment.

B. Compressible-ion model

In order to understand how the CIM representation of the short-range anion-cation interactions changes the relative crystal energetics the first step is to compare the EPP results with the CIM with no polarization effects.

The two curves of energy versus volume for the fluorite structure are identical (to within the quality of the fit) when

related to the same thermodynamic standard. There is a small deviation at very small volume ($< 23\text{ \AA}^3$) due to the simple Born-Mayer exponential being a poorer representation of the *ab initio* data in the low- R region. This is not important for the calculations as this range of R values is only sampled at very high pressures. A useful way of assessing the effect of the compressible-ion representation is to compare all polymorph energetics relative to the fluorite energy minimum.

Figure 5 shows the crystal energy against volume curves for the CIM with no polarization effects. The energetic order is now $U^{\text{fluorite}} < U^{\text{cotunnite}} < U^{\text{monoclinic}} < U^{\alpha\text{-PbO}_2} < U^{\text{rutile}}$. The effect of the CIM is to stabilize the higher coordinate structures (here the monoclinic over the $\alpha\text{-PbO}_2$) with respect to the EPP. The same effect appeared in calculations on MgO and CaO (Ref. 37) and CsCl.⁴⁰ The precise reasons for this will be analyzed in the Discussion.

The energy difference between the rutile and $\alpha\text{-PbO}_2$ structures remains approximately constant in going from the EPP ($\approx 33.9\text{ kJ mol}^{-1}$) to the CIM ($\approx 37.1\text{ kJ mol}^{-1}$) as both are based on the packing of MO_6 octahedra. The $\alpha\text{-PbO}_2$ structure is slightly stabilized by the CIM by virtue of the distortion to give a cation which is six coordinated, but which has two additional anion neighbors at a slightly greater distance, as discussed in the Introduction.

To summarize, therefore, the CIM representation of the anion-cation short-range interactions behaves very differently to the EPP in terms of the transferability to coordination numbers away from the original structure on which the models were parametrized (in this case the fluorite). Although it is gratifying that the energy minimum of the experimentally observed monoclinic phase becomes more negative than that of the $\alpha\text{-PbO}_2$ phase favored by the EPP, the story is far from complete as the fluorite structure is now the ground state predicted by the CIM. As we shall see, the inclusion of induction effects resolves this problem.

We now investigate the importance of the dipole and quadrupole terms by adding them systematically to the CIM. The dipolar part of the potential model is much better de-

TABLE VI. Crystal energy differences (in kJ mol^{-1}) with respect to the fluorite minimum for the CIM with no polarization, dipole polarization only, and both dipole and quadrupole polarization.

Structure	$V/\text{\AA}^3$			$\Delta U/\text{kJ mol}^{-1}$		
	CIM (no pol.)	CIM ($+\mu$)	CIM ($+\mu+\theta$)	CIM (no pol.)	CIM ($+\mu$)	CIM ($+\mu+\theta$)
Monoclinic	38.58	38.42	35.74	187.6	158.4	-32.3
Rutile	43.40	43.25	39.60	282.1	235.8	-23.4
Cotunnite	32.62	32.57	32.36	161.0	104.3	87.8
αPbO_2	42.00	41.64	37.99	245.0	233.4	-8.7

TABLE VII. Crystal volumes for the monoclinic structure from experiment, the DC shell model, the PIB, and the current EPP and CIM.

	$V/\text{\AA}^3$	Ref.
Eخت.	35.59	20
Eخت.	35.06	63
DC shell model	35.89	25
PIB	37.45	30
Current EPP, no polarization	35.99	-
Current EPP, dipoles only	35.90	-
Current CIM, no polarization	38.58	-
Current CIM, dipoles only	38.42	-
Current CIM, full polarization	35.74	-

finned because it has been obtained from *ab initio* calculations, whereas the quadrupolar part has been parametrized in a much more speculative fashion.

The energies with respect to the fluorite phase are given in Table VI. The dipole polarization energies range from ≈ 50 kJ mol^{-1} in the cotunnite and rutile phases to ≈ 10 kJ mol^{-1} in the α - PbO_2 polymorph. The quadrupole stabilization energies are of the order of 250 kJ mol^{-1} for the α - PbO_2 and rutile structures, 190 kJ mol^{-1} for the monoclinic, and only ≈ 10 kJ mol^{-1} for the cotunnite. The structural reasons for these energy magnitudes will be discussed in Sec. VI.

Figure 6 shows the CIM energy/volume curves for the full dipolar and quadrupolar model. Again, the fluorite curve is identical to that in Fig. 5. The relative energetics (given in Table VI) have changed dramatically with respect to the previous models. The monoclinic structure is now the ground state with the overall order $U^{\text{monoclinic}} < U^{\text{rutile}} < U^{\alpha\text{-PbO}_2} < U^{\text{fluorite}} < U^{\text{cotunnite}}$.

Table VI lists the equilibrium volumes for the various polymorphs at the energy minima. The effect of the dipole and quadrupole polarization is to increase the system densities. The largest volume changes are observed when quadrupoles are added to the α - PbO_2 , rutile and monoclinic forms, consistent with these structures having the larger quadrupole polarization energies. Table VII lists the volumes of the monoclinic structure for the various models compared with previous model results and two experimental values. The CIM without polarization effects gives a volume significantly greater than the experimental value. When *both* dipole and quadrupole effects are added the CIM molar volume decreases to give a much better agreement with experiment.

TABLE VIII. Fluorite elastic constants and bulk modulus for the current EPP and the CIM with and without full dipolar and quadrupolar polarization effects.

	B/GPa	C_{11}/GPa	C_{12}/GPa	C_{44}/GPa
EPP	201	414	95	99
CIM (no polarization)	204	405	104	471
CIM (full polarization)	204	402	105	177
Eخت. (Ref. 64)	194	417	82	47

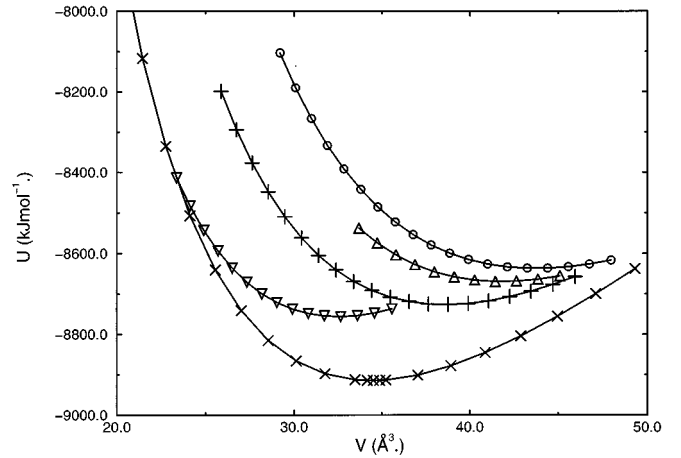


FIG. 5. Lattice energy vs volume for the CIM with no polarization effects. Key as for Fig. 4.

Although the predicted ground state is now monoclinic, in agreement with experiment, the calculated lattice energy is still significantly more positive than the experimental value.

Table VIII lists the bulk modulus and elastic constants calculated as described in the previous section. B is identical in the CIM with and without polarization effects as such effects are precluded by symmetry. C_{11} and C_{12} show a small change on the inclusion of polarization. C_{44} , however, is greatly altered by the inclusion of anion quadrupoles as a field gradient is developed by the shearing distortion. In the absence of anion quadrupoles C_{44} is much greater than the experimental value. The addition of the anion quadrupoles lowers C_{44} although it is still significantly greater than experiment.

C. Tetragonal distortion

For the tetragonal distortion the ideal fluorite structure corresponds to a local energy maximum within a double-well structure in the energy/distortion curve in which the two energy minima corresponding to the tetragonal structure. There are three parameters of general interest: the c/a ratio of the unit cell, the energy ΔU^{tet} required to mount the central energy barrier in the double-well structure, and the displacement d_z of the oxide sublattice from the ideal fluorite posi-

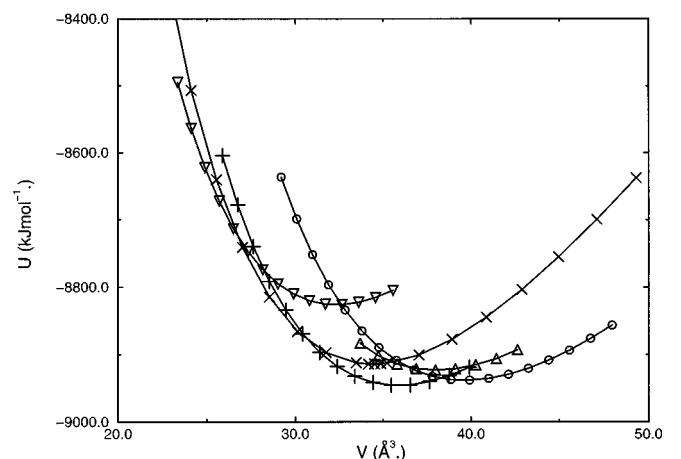


FIG. 6. Lattice energy vs volume for the CIM with full polarization effects. Key as for Fig. 4.

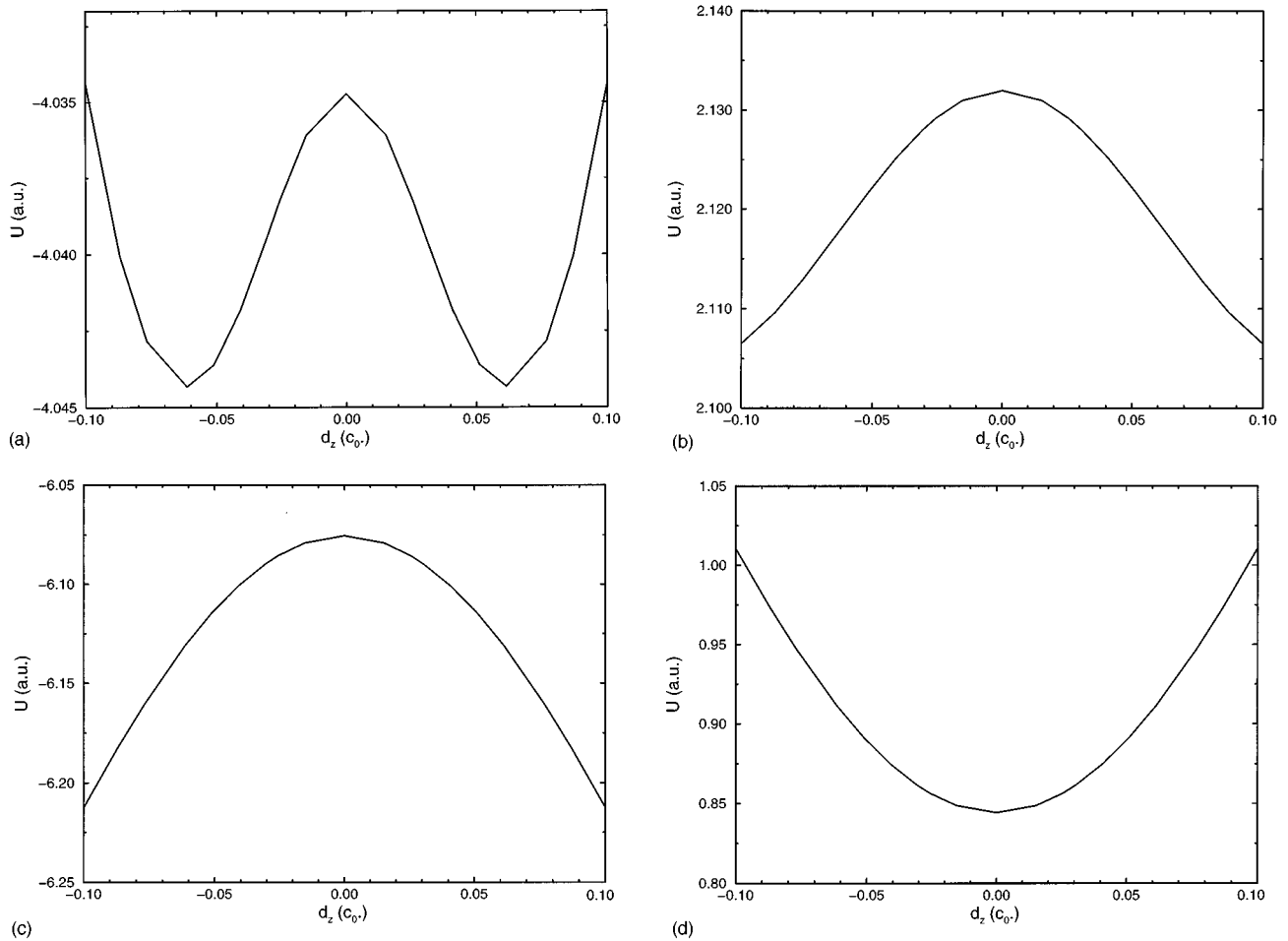


FIG. 7. Breakdown of the tetragonal distortion energy for the DC potential: (a) Total energy, (b) O-O Coulombic energy, (c) Zr-O Coulombic energy, and (d) Zr-O short-range energy.

tions in the energy minimum. The latter is usually quoted in terms of the c -axis length which, by convention, is the axis along which the oxide ions move in the distortion.

We first consider how a simple EPP can reproduce the tetragonal distortion. As before, our strategy is designed to determine the role of the various contributions to the total energy. In order to make the connection to previous empirical models both the DC potential and current EPP will be analyzed.

Figures 7(b)–7(e) show the various contributions to the total crystal energy [Fig. 7(a)] for the DC potential as a function of d_z , with cell volume corresponding to the tetragonal energy minimum throughout. No polarization phenomena are included here. The total energy shows the characteristic double-well structure discussed above. It is interesting to note that this structure appears *without* polarization effects. Polarization effects would be expected to become significant away from $d_z=0$ (where they are precluded by the high symmetry of the anion site) and so we might have expected that they alone were responsible for the double-well structure. In Figs. 7(b)–7(e) we see that the Coulombic and short-range Zr^{4+} - O^{2-} interactions effectively cancel over the d_z range of interest. The difference in O^{2-} - O^{2-} dispersion energy (there is no Zr-O term in the DC potential) is less significant than the other terms shown. The double-well structure can, therefore, be traced directly to the reduction in

O^{2-} - O^{2-} repulsive Coulombic energy that results from the tetragonal distortion. This is perhaps not such a surprising result in view of the short O^{2-} - O^{2-} nearest-neighbor length which has already been noted in the Introduction. As d_z increases from zero the anions move away from the ideal fluorite packing into a pseudo-close-packed arrangement of lower energy.

For larger cell volumes, corresponding to the density of the transition temperature, the O^{2-} - O^{2-} interaction energy is smaller as a result of the lower system density. The relatively small size of the Zr^{4+} cation compared to cations having fluorite ground states means that as d_z increases from zero the Coulombic energy gained from the decrease of two Zr-O distances *outweighs* the increase associated with the short-range repulsion. For a larger cation the potential energy minima will be at $d_z=0$ as any distortion leads to the short-range energy outweighing the Coulombic attractive force. The Zr^{4+} can be thought of as able to “rattle” in the tetrahedral hole. The result is the same double-well structure as observed at zero K.

The sum of the terms leads to the double-well structure of Fig. 7(a) with an energy minimum at $d_z \approx 0.06$. The current EPP, whose parametrization was not based on any knowledge of the nature of the tetragonal distortion, gives a different result, with $d_z > 0.1$ in poor agreement with *both* the *ab*

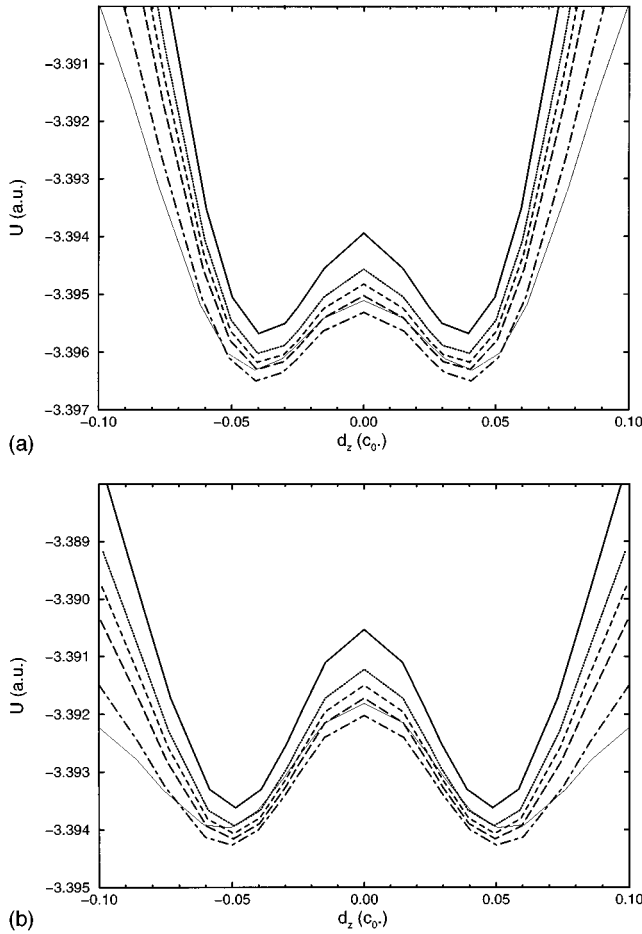


FIG. 8. CIM tetragonal distortion, full polarization. (a) at V_0 , (b) at a density corresponding to the high-temperature experimental data (Ref. 17). Key: thick solid line, $c/a=1.48$; dotted line, 1.46; dashed line, 1.45; long dashed line, 1.44; dot-dashed line, 1.42; thin solid line, 1.40.

initio and experimental data. The difference in performance of the two pair potentials can be traced back to two terms. First, the $O^{2-}-O^{2-}$ short-range energy, which reinforces the Coulombic repulsion [Fig. 7(b)], is much more significant in the EPP due to its longer range. Second, the presence of $Zr^{4+}-O^{2-}$ dispersion introduces terms that act like Fig. 7(c) with respect to d_z . Both of these terms act to increase the d_z at which the energy minimum occurs.

For the CIM, in contrast to the EPP, no double-well structure is present in the absence of polarization effects. As d_z increases from zero two anion-cation separations are reduced and two are increased—each anion becomes effectively 2+2 coordinate. As a result of this effective *lowering* of the anion coordination number the EPP *underestimates* the anion-cation short-range interaction energy in the manner already observed.

Just as for the structural energies described in Sec. V B, the inclusion of polarization effects at a purely dipolar level is not enough to reproduce the observed experimental trends, in this case the double-well structure. Figure 8(a) shows an energy against d_z plot for the full CIM (i.e., with dipoles and quadrupoles). The inclusion of anion quadrupoles (unchanged from Sec. V B) recovers the double-well structure.

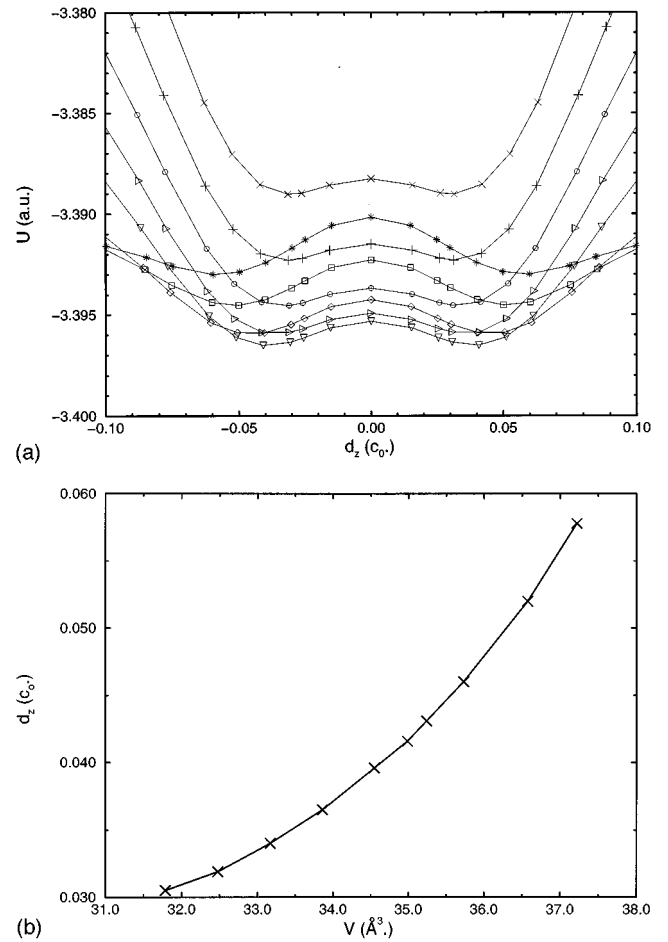


FIG. 9. (a) Tetragonal distortion using the full CIM at different volumes for $c/a=1.42$. The volumes (in a.u.) are X, 427.0; +, 436.3; \circ , 445.6; \triangleright , 454.9; ∇ , 464.2; \diamond , 480.0; \square , 491.3; *, 500.0. (b) Position of the d_z minimum against volume.

Figure 8(b) shows the same curves calculated at the density of the tetragonal-cubic transition. Figure 9(a) shows a series of energy curves for $c/a=1.42$ at differing volumes. The minimum in d_z is seen to have moved to a higher value (with respect to the zero K structure) in a manner consistent with the combined *ab initio* and experimental observations. Figure 9(b) shows the position of the d_z minimum plotted against cell volume for $c/a=1.42$. The dependence of the minimum position on volume is slightly greater than linear.

As the volume increases, in the CIM, the c/a ratio in the energy minimum remains at around 1.42. Our LMTO calculations on the other hand, show a change from a minimum at 1.42 at $V/V_0=0.92$ to a minimum at 1.44 at $V/V_0=0.96$. This increase in c/a ratio is consistent with other *ab initio* calculations and the experimental value. As the volume increases the CIM does stabilize $c/a=1.44$ over $c/a=1.40$ (at $V/V_0=1.0$) and $c/a=1.45$ over $c/a=1.40$ (at $V/V_0=1.06$). However, the overall minimum remains at $c/a=1.42$ in conflict with the experimental observation. In other words we can state that the general trend towards the smaller c/a ratio being destabilized with increasing volume is reproduced by the CIM but the effect is not large enough to stabilize $c/a=1.45$ at the experimental high-temperature density. Possible reasons for this shortcoming will be described in Sec. VI.

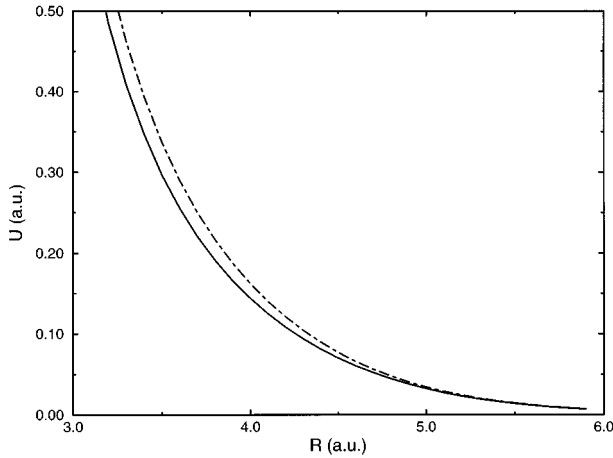


FIG. 10. EPP's derived for three-coordinate (dashed line) and four-coordinate (solid line) anions.

As the volume increases, the height of the energy barrier about $d_z=0$ increases. The LMTO calculations give energy barriers in the range from 0–1 a.u. at $V/V_0=0.92$ to 1.5–3.5 a.u. at $V/V_0=0.98$. The CIM gives a barrier height of ≈ 0.75 a.u. at $V/V_0=0.92$, increasing to ≈ 2.1 a.u. at $V/V_0=1.06$ (corresponding to the high-temperature density). Hence, the general trends in both barrier height and behavior with volume are reproduced.

VI. DISCUSSION

A. Transferability of the CIM

The most important aspect of the CIM representation of the anion-cation short-range interaction is the stabilization of higher-coordinate structures. For ZrO_2 the seven-coordinate monoclinic structure is stabilized over the six-coordinate $\alpha\text{-PbO}_2$ structure. The $\alpha\text{-PbO}_2$ structure is not observed in ZrO_2 , but it tends to appear in systems with increasing cation size, as the ionic model predicts. For example, several of the systems in the structure map of Table I with the rutile ground state undergo a pressure driven transition to the $\alpha\text{-PbO}_2$ structure. In addition, the mixed cation ZrTiO_4 system forms a high-temperature $\alpha\text{-PbO}_2$ phase.⁵⁹ At lower temperatures this structure distorts to allow the Zr^{4+} cation to attain near-eightfold coordination with the smaller Ti^{4+} becoming sixfold coordinated.

The observation that the CIM stabilizes the higher-coordinate structures has also been made for MgO , CaO ,³⁷ and CsCl .⁴⁰ We believe it is a general result, which we can illustrate by the following example. Let us construct a new EPP corresponding to a three-coordinate anion crystal structure. The CIM potential (fitted to the four-coordinate *ab initio* data) is used to produce the three-coordinate curves which are then used to generate the new EPP in the same manner as before. Thus,

$$U_3^{\text{SR}}(R) = \sum_{i=2}^{N_i} \sum_{j=1}^{i-1} U_3^{\text{EPP}}(r^{ij}) = \frac{1}{3} [U_3^{\text{re}}(R) - U_3^{\text{re}}(\infty)] + U_3^{\text{ov}}, \quad (6.1)$$

where U_3^{re} and U_3^{ov} are now the rearrangement and overlap energies in the three-coordinate structure. Figure 10 shows the comparison of the EPP derived from the four-coordinate (*ab initio*) data (EPP-4) with that derived from the three-coordinate CIM (EPP-3). If the EPP representation of the short-range interactions were truly transferable, these curves would be identical. However, EPP-3 is consistently more repulsive than EPP-4 over the range of anion-cation separations of interest. The repulsive energy stored in a compressed anion increases less than linearly with the number of neighbors compressing it. Hence, the use of EPP-4 to model all polymorphs leads to the anion-cation repulsive energy being *underestimated* for structures with coordination number less than 4 and *overestimated* for coordination numbers greater than 4. The CIM stabilizes higher-coordinate structures (and destabilizes lower-coordinate systems) with respect to the EPP.

Previous CIM work on MgO clearly demonstrates the greater transferability of the CIM representation by comparing it with additional *ab initio* calculations.³⁷ In that case the CIM was fitted to a six-coordinate rocksalt structure and then used to generate the four- and eight-coordinate U^{re} and U^{ov} . These curves compared excellently with additional *ab initio* calculations on the four- and eight-coordinate structures (which had not been used to parametrize the CIM in any way), demonstrating the true transferability.

B. Dipoles and quadrupoles

The second important aspect of our investigation concerns the magnitude of the polarization energies. The dipole polarization energies are small compared to those found in, for example, layered structures⁶⁰ where the anions sit in highly asymmetric environments. Such layered structures become stabilized for combinations of small (highly polarizing) cations and large (highly polarizable) anions. As a result of the relatively small dipole polarizability of the oxide anion such structures are not observed for this series (analogous to the halide case in which no such structures are formed by fluorides but dominate the other halide systems). In the polymorphs considered here the anions are in sites at which large dipolar induction effects are precluded by the high symmetry. The small dipoles that do arise do so as a result of small displacements of the anions from the ideal lattice sites. As a result the dipole polarization effects are not nearly large enough to stabilize the monoclinic structure over the fluorite in the CIM.

The quadrupole stabilization energy for the rutile, $\alpha\text{-PbO}_2$, and monoclinic phases is much larger than the corresponding dipole energy. This behavior can be traced back to the existence of the three-coordinate oxide sites which result in significant field *gradients* which give rise to the relatively large quadrupoles. The quadrupole stabilization energy is similar for $\alpha\text{-PbO}_2$ and the rutile phases as both are based exclusively on the three-coordinate oxide sites, although the $\alpha\text{-PbO}_2$ energy is slightly smaller due to the distortion of the oxide site to the effective 3+1 coordination. The monoclinic quadrupole stabilization energy is considerably less than that for either the rutile or the $\alpha\text{-PbO}_2$ structures but still much greater than the dipole polarization energy. This can be traced back to the ‘‘intermediate’’ nature

of the monoclinic structure discussed previously in which the anions occupy alternating layers of three-coordinate (rutile) and four-coordinate (fluorite) sites. Thus, half the anions lie in the three-coordinate sites which lead to the large quadrupole effects, while the other half lie in the more symmetric four-coordinate sites. Despite only half the anions now being in the critical three-coordinate sites the overall quadrupole stabilization energy is over half that of the rutile, as there is a significant distortion of the local tetrahedra of cations around the four-coordinate sites.

An interesting side issue is that this observed role for anion quadrupoles has implications for the effective modeling of systems which themselves have rutile as their ground-state structure, for example, TiO_2 itself. This is a traditionally difficult simulation problem, with current models either reproducing the experimental structure *or* the dielectric properties but not both simultaneously.⁶¹ Future work will test if the current developments help to rectify this situation.

C. Cancellation of errors

The available empirical models and, indeed, the current EPP all appear to do a satisfactory job of modeling *certain aspects* of the behavior of ZrO_2 . For example, these models *do* stabilize the monoclinic structure over the fluorite and give good agreement with the experimental and theoretical molar volumes. However, they are stuck with the fundamental problem of the stability of the $\alpha\text{-PbO}_2$ structure. Similarly, the empirical potentials appear to model the tetragonal distortion relatively well although the agreement with the *high-temperature* experimental data appears better than that with the 0 K *ab initio* calculations. However, the current CIM (derived from *ab initio* calculations) gives poor agreement with both the experiment and the *ab initio* tetragonal calculations. The effectiveness of the pair potentials in modeling specific aspects of the structure can be attributed to an effective cancellation of errors. The CIM, without polarization effects, gives the monoclinic structure equilibrium volume as significantly greater than both the experiment and the EPP prediction and shows no double-well structure for the tetragonal distortion. The addition of *both* dipole and quadrupole polarization effects rectifies both of these problems; with this full CIM the monoclinic equilibrium volume is lowered to give good agreement with experiment and the double-well structure returns. Thus, the partial successes of the pair potentials appear in cases where the compressibility and quadrupole effects effectively cancel. Importantly, the full CIM now gives the monoclinic structure as the ground state *and* predicts tetragonal distortions in better agreement with both the *ab initio* and experimental data.

A further manifestation of this cancellation of errors is seen in the elastic constant C_{44} . The EPP gives good agreement with experiment, while the CIM, without polarization effects, upsets the cancellation of errors and predicts a C_{44} an order of magnitude too large. The inclusion of the anion quadrupole effects returns the agreement with experiment although, in this case, the agreement is slightly worse for the CIM than for the EPP. This will be developed later in this section.

D. Other terms in the potential model

The role of the $\text{O}^{2-}\text{-O}^{2-}$ short-range term has also been found to be critical. Previous models have favored the use of an empirical potential.⁶² The current work uses a potential fitted to *ab initio* calculations using the oxide anion electron density appropriate to the equilibrium lattice parameter (a “frozen” potential). Although the *energy* of even the current potential is much less than the corresponding Coulombic repulsive energy at the typical crystal separations, it is the *curvature* of the short-range curve that is important and that effects the crystal properties. The general effect is to destabilize the higher-coordinate structures. The greater the number of anions packed around a central cation, the smaller the anion-anion nearest-neighbor separations tend to be. For example, the experimental nearest-neighbor anion-anion separations lie in the range 2.581–2.985 Å,²¹ while the current models give 2.581 Å as the fluorite analog for *all* nearest-neighbor pairs. The reduction of cation-anion coordination number from 8 to 7 allows a relaxation in the cation first-coordination sphere.

E. Shortcomings and future development

The current model is, of course, far from perfect. Shortcomings are observed in both the modeling of the tetragonal phase and the C_{44} elastic constant in the fluorite structure. The predicted increase in the c/a ratio at the energy minima from ≈ 1.42 at small volume to ≈ 1.45 at the high-temperature density is not observed, although a trend towards an increase in the c/a ratio with increased molar volume is seen. Similarly, although the effect of the quadrupole polarization is to lower C_{44} towards the experimental value, the final value is higher than that observed experimentally. Again, however, the correct trend is present.

Both of these shortcomings may be related to the relatively speculative manner in which the quadrupolar aspects of the model have been parametrized. The short-range, dipolar induction, and dispersion effects (including damping) are all fixed to *ab initio* calculations and, as such, are well defined. The full quadrupole CIM model could, in theory, account for *both* Coulombic- and overlap-induced quadrupoles in a manner analogous to the dipoles, using *ab initio* data. However, the lack of data leads to our using a *smaller* quadrupole polarizability than would be expected in order to mimic the damping effect of the overlap on the Coulombic-induced moment. In the tetragonal phase and the calculation of C_{44} the role of the quadrupoles is particularly subtle and so the shortcomings of this approximation may become exposed.

VII. CONCLUSIONS

Previous models of the ionic type, including the shell model, are unable to predict the stability of the ground-state monoclinic structure of ZrO_2 with respect to an orthorhombic structure. Our aim has been to understand the origin of this problem and to develop an improved, physically based model. In the process of doing this we have obtained a better general understanding of the origin of the observed crystal structures in the metal dioxides.

We have investigated systematically the energetics of sev-

eral crystal structures of ZrO_2 using a range of semiempirical interatomic potentials. The three structures which are observed at increasing temperatures are monoclinic, tetragonal, and cubic (fluorite). Besides these we have studied hypothetical structures which some potentials erroneously predict or which occur in other oxides, e.g., the α - PbO_2 structure or rutile.

The first important effect we have included is spherical relaxation ("breathing") of the oxygen ion. This is the compressible ion model (CIM). The ion contracts as its coordination increases, resulting in a reduction in overlap energy but an increase in rearrangement energy. It is therefore a more repulsive object (with lower rearrangement energy) at lower coordination. However, the reduction in rearrangement energy is not offset by the gain in overlap energy. The result of this is to destabilize lower-coordination structures; in particular the six-coordinate α - PbO_2 structure is thereby brought to a higher energy than the experimentally observed seven-coordinate monoclinic structure. An effective pair potential (EPP) cannot achieve this by any amount of fitting, because an EPP is fundamentally not transferable.

However, the CIM is also found to stabilize the eight-coordinate fluorite over both the six- and seven-coordinate polymorphs. We find that the addition of anion polarization at *both* the dipolar and quadrupolar levels is necessary in order to stabilize the seven-coordinate monoclinic structure. The stabilization works because the anions sit in much more asymmetric environments in the monoclinic than in the fluorite structure. We can picture the seven-coordinate monoclinic structure as consisting of alternating layers of rutilelike three-coordinate oxygen ions and fluoritelike four-coordinate oxygen ions. The driving force for the formation of this structure appears to be the existence of the three-coordinate

oxygen sites, which are the sites that experience the largest quadrupole polarization.

Besides the various perfect crystal structures, we have investigated the energy pathway for distortion of the cubic to the tetragonal structure. The experimental data point to the existence of a double well in the energy versus tetragonal distortion of the oxygen sublattice. Although this is reproduced with an EPP, it is for the wrong reason, due to a fortuitous cancellation of errors. A CIM, even with dipole polarizability, shows no double well. It is only properly accounted for when quadrupole distortions of the anions are included.

We have found that although some structural information can *apparently* be explained with a simple ionic or shell model, these models are not transferable. The CIM with dipolar and quadrupolar terms is necessary in order to explain all the data we have from experiment and *ab initio* calculations. We can therefore apply it with some confidence to study thermal properties such as phase transitions and defects such as grain boundaries.

ACKNOWLEDGMENTS

We thank John Harding and Nick Pyper for supplying details of their *ab initio* calculations, and for discussions and help in general. We are grateful to Paul Madden for useful discussions about interatomic forces in ionic materials. M.W. is grateful for support from the Alexander von Humboldt Foundation. U.S. thanks the Deutsche Forschungsgemeinschaft for support under Grant No. Fi478/1-2. This work has benefited from collaborations within, and has been partially funded by, the E.U. Human Capital and Mobility Network on "Ab initio calculation of complex processes in materials" (Contract No. ERBCHRXCT930369).

*Present address: School of Mathematics and Physics, The Queen's University, Belfast BT7 1NN, Northern Ireland.

¹*Science and Technology of Zirconia*, Advances in Ceramics, Vol. 3, edited by A. H. Heuer and L. W. Hobbs (The American Ceramic Society, Columbus, OH, 1981); *Phase Transformations in ZrO₂-Containing Ceramics*, Advances in Ceramics Vol. 12, edited by A. H. Heuer, N. Claussen, and M. Rühle (The American Ceramic Society, Columbus, OH, 1981).

²H. J. F. Jansen, Phys. Rev. B **43**, 7267 (1991).

³R. Orlando, C. Pisani, C. Roetti, and E. Stefanovich, Phys. Rev. B **45**, 592 (1992).

⁴B. G. Dick and A. W. Overhauser, Phys. Rev. **112**, 90 (1958).

⁵M. Wilson and P. A. Madden, J. Phys. Condens. Matter, **5**, 2687 (1993).

⁶P. W. Fowler and P. A. Madden, Phys. Rev. B **29**, 1035 (1984).

⁷G. D. Mahan, Solid State Ionics **1**, 29 (1980).

⁸W. Shockley, Phys. Rev. **73**, 1273 (1948).

⁹R. W. G. Wyckoff, *Crystal Structures* (Interscience, New York, 1965).

¹⁰S. Kawasaki and T. Yamanaka, J. Mater. Sci. Lett., **13**, 514 (1994).

¹¹R. Suyama, T. Ashida, and S. Kume, J. Am. Ceram. Soc. **68**, C314 (1985).

¹²S. Block, J. A. H. Da Jornada, and G. J. Piermarini, J. Am. Ceram. Soc. **68**, 497 (1985).

¹³Y. Kudoh, H. Takeda, and H. Arashi, Phys. Chem. Min. **13**, 233 (1986).

¹⁴O. Ohtaka, T. Yamanaka, and T. Yagi, Phys. Rev. B **49**, 9295 (1994).

¹⁵O. Ohtaka, S. Kume, and E. Ito, J. Am. Ceram. Soc. **71**, C448 (1988); **73**, 744 (1990).

¹⁶O. Ohtaka, T. Yamanaka, S. Kume, E. Ito, and A. Navrotsky, J. Am. Ceram. Soc. **74**, 505 (1991).

¹⁷P. Aldebert and J-P. Traverse, J. Am. Ceram. Soc. **68**, 34 (1985).

¹⁸U. Müller, *Structural Inorganic Chemistry* (Wiley, New York, 1991).

¹⁹E. V. Stefanovich, A. L. Shluger, and C. R. A. Catlow, Phys. Rev. B **49**, 11 560 (1994).

²⁰J. D. McCullough and K. N. Trueblood, Acta. Crystallogr. **12**, 507 (1959).

²¹D. K. Smith and H. W. Newkirk, Acta Crystallogr. **18**, 983 (1965).

²²C. J. Howard, R. J. Hill, and B. E. Reichart, Acta. Crystallogr. B **44**, 116 (1988).

²³J. G. Stark and H. G. Wallace, *Chemistry Data Book*, 2nd ed. (John Murray, London, 1984).

²⁴L. L. Boyer and B. M. Klein, J. Am. Ceram. Soc. **68**, 218 (1985).

²⁵A. Dwivedi and A. N. Cormack, Phil. Mag. A **61**, 1 (1990).

²⁶General Utility Lattice Program, Julian Gale, Imperial College, London, UK, 1993.

²⁷R. Dovesi, V. R. Saunders, and C. Roetti, CRYSTAL92, User's Manual (Gruppo di Chimica Teorica, Università di Torino and SERC Daresbury Lab., 1992).

- ²⁸A. L. Shluger and E. A. Kotomin, *Phys. Status Solidi B* **108**, 673 (1981).
- ²⁹L. L. Boyer, M. J. Mehl, J. L. Feldman, J. R. Hardy, J. W. Flocken, and C. Y. Fong, *Phys. Rev. Lett.* **54**, 1940 (1985).
- ³⁰R. E. Cohen, M. J. Mehl, and L. L. Boyer, *Physica B* **150**, 1 (1988).
- ³¹R. J. Ackermann, E. G. Rauh, and C. A. Alexander, *High Temp. Sci.* **7**, 304 (1975).
- ³²P. W. Fowler and P. A. Madden, *J. Phys. Chem.* **89**, 2581 (1985).
- ³³N. C. Pyper, *Philos. Trans. A* **320**, 107 (1986).
- ³⁴N. C. Pyper, *Proc. R. Soc. London A* **352**, 89 (1995).
- ³⁵N. C. Pyper, *Adv. Solid. State Chem.* **2**, 223 (1991).
- ³⁶G. D. Mahan and K. R. Subbaswamy, *Local Density Theory of Polarizability* (Plenum, London, 1990).
- ³⁷M. Wilson, P. A. Madden, N. C. Pyper, and J. H. Harding, *J. Chem. Phys.* **104**, 8068 (1996).
- ³⁸J. H. Harding (unpublished).
- ³⁹J. H. Harding and N. C. Pyper, *Philos. Mag. Lett.* **71**, 113 (1995).
- ⁴⁰N. C. Pyper, *Chem. Phys. Lett.* **220**, 70 (1994).
- ⁴¹W. H. Press, B. P. Flannery, S. A. Teukolsky, and W. T. Vetterling, *Numerical Recipes* (Cambridge University Press, Cambridge, England, 1986).
- ⁴²M. Sprik and M. L. Klein, *J. Chem. Phys.*, **89**, 7556 (1988).
- ⁴³R. Car and M. Parrinello, *Phys. Rev. Lett.* **55**, 2471 (1985).
- ⁴⁴P. W. Fowler and P. A. Madden, *Phys. Rev. B* **31**, 5443 (1985).
- ⁴⁵K. T. Tang and J. P. Toennies, *J. Chem. Phys.* **80**, 3726 (1984).
- ⁴⁶M. Wilson, B. J. C. Cabral, and P. A. Madden, *J. Phys. Chem.* **100**, 1227 (1996).
- ⁴⁷M. Rühle and A. H. Heuer, *Adv. Ceram.* **12**, 14 (1984).
- ⁴⁸P. W. Fowler, J. H. Harding, and N. C. Pyper, *J. Phys. Condens. Matter* **6**, 10 593 (1994).
- ⁴⁹W. C. Mackrodt and P. M. Woodrow, *J. Am. Ceram. Soc.* **69**, 277 (1986).
- ⁵⁰W. R. Johnson, D. Kolb, and K. N. Huang, *At. Data Nucl. Data Tables* **28**, 333 (1983).
- ⁵¹P. W. Fowler and N. C. Pyper, *Proc. R. Soc. London A* **398**, 377 (1985).
- ⁵²H. M. Kelly and P. W. Fowler, *Mol. Phys.* **80**, 135 (1993).
- ⁵³M. V. K. Sastri, P. L. Narasimhulu, and K. D. Sen, *J. Chem. Phys.* **80**, 584 (1983).
- ⁵⁴K. D. Sen, *J. Phys. C* **17**, L227 (1984).
- ⁵⁵J. C. Slater and J. G. Kirkwood, *Phys. Rev.* **37**, 682 (1931).
- ⁵⁶G. Starkschall and R. G. Gordon, *J. Chem. Phys.* **56**, 2801 (1972).
- ⁵⁷N. Jacobi and Gy Csanak, *Chem. Phys. Lett.* **30**, 367 (1975).
- ⁵⁸D. C. Wallace, *Thermodynamics of Crystals*, (Wiley, New York, 1972).
- ⁵⁹R. Christoffersen and P. K. Davies, *J. Am. Ceram. Soc.* **75**, 563 (1992).
- ⁶⁰M. Wilson and P. A. Madden, *J. Phys. Condens. Matter* **6**, 159 (1994).
- ⁶¹C. R. A. Catlow, C. M. Freeman, M. S. Islam, R. A. Jackson, M. Leslie, and M. Tomlinson, *Phil. Mag. A* **58**, 123 (1988).
- ⁶²C. R. A. Catlow, *Proc. R. Soc. London A* **333**, 533 (1977).
- ⁶³J. Adam and M. D. Rogers, *Acta. Crystallogr.* **12**, 951 (1959).
- ⁶⁴H. M. Kandil, J. D. Greiner, and J. F. Smith, *J. Am. Ceram. Soc.* **67**, 341 (1984).